IRE1-UBE2D3 signaling controls the recruitment of myeloid cells to glioblastoma.

Joanna Obacz[1,2], Jérôme Archambeau[1,2], Pierre Jean Le Reste[1,2,3,12], Raphael Pineau[1,2], Florence Jouan[1,2], Kim Barroso[4,5,6,7], Efstathios Vlachavas[8,11,13], Konstantinos Voutetakis[11,12], Tanya Fainsod-Levi[9], Akram Obiedat[10], Zvi Granot[9], Boaz Tirosh[10], Juhi Samal[14], Abhay Pandit[14], John Patterson[15], Qinping Zheng[16], Luc Négroni[4,5,6,7], Aristotelis Chatziioannou[8,11], Véronique Quillien[1,2,17*], Tony Avril[1,2,17] and Eric Chevet[1,2,17*]

[1]Inserm U1242, University of Rennes, Rennes, France. [2]Centre de lutte contre le cancer Eugène Marquis, Rennes, France. [3]Neurosurgery dept, University Hospital of Rennes, 35000 Rennes, France. [4]Institut de Génétique et de Biologie Moléculaire et Cellulaire, 67404 Illkirch, France. [5]Centre National de la Recherche Scientifique, UMR7104, 67404 Illkirch, France. [6]Institut National de la Santé et de la Recherche Médicale, U1258, 67404 Illkirch, France. [7]Université de Strasbourg, 67404 Illkirch, France. [8]e-NIOS PC, Kallithea-Athens, Greece. [9]Department of Developmental Biology and Cancer Research, Institute for Medical Research Israel-Canada, Hebrew University Medical School, Jerusalem, Israel. [10]Institute for Drug Research, School of Pharmacy, Faculty of Medicine, Hebrew University of Jerusalem, Jerusalem, Israel. [11]Institute of Biology, Medicinal Chemistry and Biotechnology, NHRF, Athens, Greece. [12]Department of Biochemistry and Biotechnology, University of Thessaly, Larissa, Greece. [13]Department of Molecular Biology and Genetics, Democritus University of Thrace, 68100 Dragana, Greece. [14] CÚRAM, Centre for Research in Medical Devices, National University of Ireland, Galway, Ireland. [15]Fosun Orinove PharmaTech Inc., 3537 Old Conejo Road, Suite 104, Newbury Park, CA 91320, USA. [16]Fosun Orinove PharmaTech Inc., Suite 211, Building A4, 218 Xinghu St., Suzhou Industrial Park, Jiangsu 215123, China. [17]Rennes Brain Cancer Team (REACT), 35000 Rennes, France.

Running title: tumor IRE1-dependent inflammation

Keywords: Unfolded Protein Response, proteostasis, inflammation

*Correspondence to: Eric Chevet (eric.chevet1@gmail.com) or Véronique Quillien (v.quillien@rennes.unicancer.fr) - INSERM U1242, “Chemistry, Oncogenesis, Stress, Signaling”, Universite de Rennes 1, Centre de Lutte Contre le Cancer Eugene Marquis, Avenue de la bataille Flandres Dunkerque, 35042 Rennes, France.

Abstract

Many intrinsic and environmental stresses trigger the accumulation of misfolded proteins in the endoplasmic reticulum (ER), leading to ER stress. This condition has been observed in various human diseases, including cancer. As such, glioblastoma multiforme (GBM), the most aggressive and lethal primary brain tumor, was reported to present features of ER stress and to depend on ER stress signaling to sustain growth. Tumor cells can also use unfolded protein response (UPR) signaling to acquire malignant features thereby promoting tumor progression. IRE1 is a central mediator of the UPR, whose RNase activity leads to the non-conventional splicing of XBP1 mRNA and RNA degradation through Regulated IRE1 dependent decay (RIDD). We recently showed that IRE1 activity in GBM promotes tumor invasion, angiogenesis and infiltration by macrophages. Hence, high tumor IRE1 activity predicted worse outcome *in vivo*. Herein, we further characterize the IRE1-dependent signaling mechanism that shapes the brain tumor immune microenvironment, in particular towards myeloid cells. The latter phenomenon is mediated in part by IRE1-dependent regulation of CXCL2, IL6 and IL8 expression. We further found that IRE1 through the XBP1s transcriptional activity induces the expression of E2 ubiquitin enzyme UBE2D3, which in turn promotes inflammation. We show that UBE2D3 triggers the recruitment of myeloid cells to tumors *in vitro* and *in vivo* by targeting the NFKB signaling inhibitor, IKB leading to the up-regulation of pro-inflammatory chemokines expression. Our work identifies a novel IRE1/UBE2D3 signaling axis that plays an instrumental role in the immune regulation of glioblastoma.

INTRODUCTION

Perturbation of endoplasmic reticulum (ER) homeostasis (also known as proteostasis) is one of the hallmarks of highly proliferative or secretory cells. Moreover, many intrinsic and environmental pressures, such as low oxygen levels, acidification or nutrients shortage may also increase the risk of misfolded proteins accumulation within the ER lumen, generating so called ER stress. IRE1 is the most conserved regulator of cell response to ER stress that together with the ER transmembrane proteins PERK and ATF6 triggers activation of the unfolded protein response (UPR). UPR aims at alleviating the ER stress or inducing apoptosis when cell faces the irremediable damages (Chen and Brandizzi, 2013; Chevet et al., 2015; Dufey et al., 2014; Maurel et al., 2015). Once activated, IRE1 that harbors the serine/threonine kinase and ribonuclease (RNase) activities dimerizes/oligomerizes, which induces three major downstream pathways: JNK1 (Han et al., 2009), XBP1 mRNA splicing (XBP1s) (Calfon et al., 2002) and Regulated IRE1 dependent decay (RIDD) of RNA (Hollien and Weissman, 2006; Maurel et al., 2014). The XBP1s acts as a transcriptional regulator of genes involved in protein glycosylation, ER-associated degradation, protein folding, and lipid synthesis (Almanza et al., 2018; Hetz et al., 2011), while RIDD output controls cell fate under ER stress conditions (Maurel et al., 2014). Features of ER stress and UPR hyper-activation have been observed in many pathological situations including cancer. As such, the UPR has emerged as an adaptive mechanism supporting tumor progression and resistance to treatment by impacting almost all cancer hallmarks (Urra et al., 2016). Mounting evidence also suggests that UPR shapes tumor microenvironment by regulating angiogenesis, inflammation and host immune response (Logue et al., 2018; Obacz et al., 2017b).

The consequences of UPR signaling have been studied in various cancers such as breast, liver, lung, prostate, pancreas, and in glioblastoma multiforme (GBM), one of the most lethal and aggressive primary brain tumor with a median survival of 15-18 months despite invasive multimodal treatment (Le Reste et al., 2016). IRE1 contributes to GBM development by regulating tumor growth, migration, invasion and vascularization, partially through RIDD-mediated cleavage of SPARC mRNA (Auf et al., 2010; Dejeans et al., 2012). Loss of functional IRE1 signaling is also associated with decreased expression of proangiogenic and pro-inflammatory VEGFA, IL1β, IL6, and IL8 in GBM cells (Auf et al., 2010). Importantly, we have recently shown a pivotal role of IRE1 in the immune cell infiltration and remodeling of GBM stroma, which engaged the antagonistic role of XBP1s and RIDD (Lhomond et al., 2018). However, the precise IRE1-dependent mechanisms regulating the pro-tumoral inflammation and/or immune response in GBM remain elusive. So far it has been shown in different cellular models that IRE1 induces the expression of pro-inflammatory chemokines, which occurs through both XBP1s and JNK-dependent pathways (Martinon et al., 2010; Shanware et al., 2014) or through IRE1-mediated induction of GSK3β (Kim et al., 2015). IRE1 was also

reported to interact with TRAF2, recruiting IκB kinase (IKK), which triggers the phosphorylation and degradation of IκB, enabling the NFκB nuclear translocation (Hu et al., 2006). In addition, the IRE1-TRAF2 complex was shown to induce JNK phosphorylation and subsequent upregulation of pro-inflammatory genes through activator protein 1 (AP1) (Grootjans et al., 2016; Urano et al., 2000). Given that brain malignancies are infiltrated by a large number of immune cells, which modulate GBM aggressiveness and response to treatment, here we aimed at investigating the molecular mechanisms by which IRE1 controls GBM immune/inflammatory infiltrate. We showed that IRE1 governs the reciprocal communication between cancer and non-tumoral cells of the microenvironment by promoting the recruitment of myeloid cells to GBM. This involves a novel IRE1/UBE2D3 signaling mechanism regulating NFκB activation, which leads to the production of pro-inflammatory chemokines and the subsequent recruitment of immune/inflammatory cells to the tumor site.

RESULTS

Neutrophils are recruited to GBM in an IRE1-dependent manner *in vitro* and *in vivo*

As we previously demonstrated that IRE1 activity in GBM cells controlled the recruitment of inflammatory cells such as macrophages and microglial cells (Lhomond et al., 2018), we herein sought to test whether this was also true for other cells from the myeloid lineage. To this end, we first analyzed samples from an in-house GBM cohort (n=65) for the presence of macrophages/microglia, lymphocytes and granulocytes in the GBM microenvironment. Freshly dissociated tumors were analyzed by FACS for the expression of specific markers for each cell types (**Fig. 1A and Fig. S1A**). We confirmed that macrophages/microglia constituted a majority of GBM infiltrates (Badie and Schartner, 2000), while granulocytes were found in approximately 15% of analyzed specimens (**Fig. 1A**). Next, using GBMmark transcriptome data, we identified a similar proportion of tumors with elevated neutrophils infiltration as analyzed by the expression levels of the neutrophil-specific markers CD66b, MPO, PGLYRP1, BTLN8 and CD177 (**Fig. 1B**). Finally, the presence of neutrophils in GBM specimens was evaluated using immunohistochemistry with anti-CD66b antibodies. This showed that neutrophils were present within tumor tissue and localized to different GBM sites including the proximity of blood vessels and necrotic areas (**Fig. 1C**). Since the clinical relevance of neutrophils in cancer is rather ambiguous, we exploited publicly available TCGA dataset of GBM using GlioVis tool (Bowman et al., 2017) and found that high neutrophils infiltration (based on MPO expression) is associated with poorer patient prognosis (**Fig. 1D**). This phenomenon was not observed when the infiltration by macrophage/microglial cells was taken into consideration in the same tumors (**Fig. S1B**), thus indicating a selective pro-tumoral role of neutrophils.

Using the expression of CD177 as a neutrophil marker, we showed that tumors with high IRE1 activity, as classified according to our previous study (Lhomond et al., 2018), recruited significantly higher number of neutrophils compared to IRE1 low tumors (**Fig. 1E**). This suggested that IRE1 signaling could contribute to neutrophils attraction that in turn may promote tumor aggressiveness. To further address this hypothesis, neutrophil migration was determined using Boyden chamber assays. For that, neutrophils were isolated from the blood of healthy donors and characterized based on the expression of CD14, CD15, CD66b and CD16 surface receptors (**Fig. S1C**). We also generated a GBM primary cell line RADH87 with stable overexpression of wild-type (WT) IRE1 or of a truncated IRE1 variant, Q780* (**Fig. S1D**). The latter mutation was shown to abrogate IRE1 signaling and its downstream output towards XBP1 splicing, therefore resembling the characteristics of U87 DN cells (**Fig. S1D** (Lhomond et al., 2018). As shown in **Fig. 1F-G**, tumor cells conditioned media (TCCM) derived from U87 DN and RADH87 Q780* cells did not recapitulate the migratory abilities of neutrophils in Boyden chamber assay, when compared to TCCM from parental U87 cells or

RADH87 IRE1 WT cells. Lastly, we validated the role of IRE1 activity in neutrophil recruitment *in vivo*. As such, mice were first injected with GL261 GBM cells and then 14 days post-injection, underwent surgical removal of their tumor, followed by insertion of either empty gel implant (referred to as plug) or plug containing the IRE1 inhibitor, MKC8866 (Logue et al., 2018). As a result, we showed that pharmacological abrogation of IRE1 activity with MKC8866 significantly abolished neutrophils infiltration to the recurring GBM (**Fig. 1H-I**). Overall, our results demonstrate that GBM are infiltrated by neutrophils and this is mediated at least in part by IRE1 signaling.

IRE1 activity regulates the expression of neutrophil-attracting chemokines

Based on our previous work and the above results, we hypothesized that IRE1 activity in tumor cells could control the expression of specific chemokines, resulting in the attraction of neutrophils. A number of cytokines/chemokines stimulating neutrophils attraction has been described in different cancer models, including CXCL1, CXCL2, CXCL5, IL6, IL8, IL17, and TNFα (Powell and Huttenlocher, 2016). To test whether any of those soluble factors could be responsible for promoting neutrophil recruitment to GBM, freshly isolated neutrophils were exposed to tumor cell conditioned media (TCCM) derived from various GBM cell lines (both primary and established), which as expected, resulted in significant induction of neutrophil migration through the Boyden chambers (**Fig. S2A**). We then analyzed chemokines expression in those TCCM using ELISA-based assay and found that neutrophil chemoattraction correlated with the elevated levels of CXCL1, CXCL2, IL6, IL8 and CXCL12 (**Fig. 2A-B**). Using tumor's transcriptomes from two independent cohorts, namely GBMmark and TCGA, we further demonstrated that tumors with increased neutrophils infiltration, as measured with the expression levels of MPO and CD177, expressed significantly higher levels of CXCL2, IL6 and IL8 (**Fig. 2C, Fig. S2B**). In line with our previous work (Auf et al., 2010), we showed that expression of those neutrophils attracting chemokines depended on IRE1 activity. As depicted in **Fig. 2D-E**, mRNA levels of CXCL2, IL6 and IL8 were dramatically reduced in U87 DN and RADH87 Q780* cells, both expressing inactive IRE1, when compared to control or WT-overexpressing cells. These findings indicate that IRE1 signaling is involved in the regulation of chemokines expression, which once secreted could be involved in the recruitment of neutrophils to the tumors.

UBE2D3 is a novel component of IRE1 signaling involved in the regulation of neutrophil infiltration in GBM

To decipher the IRE1-dependent mechanism of neutrophil infiltration, we next focused our attention on the molecules, whose expression i) is linked to inflammation and ii) might be regulated by IRE1 signaling including XBP1 mRNA splicing and/or RIDD. To this end, we

evaluated the expression of genes derived from our recently established categorization of tumors according to IRE1 signature (Lhomond et al., 2018), and identified the E2 ubiquitin-conjugating enzyme, UBE2D3 (also known as UbcH5c) to be one of the targets that could mediate immune cells chemoattraction. Following our aforementioned criteria, we showed that UBE2D3 expression was significantly elevated in the population of tumors with high IRE1 activity (**Fig. 3A)** and was associated with increased neutrophils infiltration, as indicated by the expression level of MPO marker (**Fig. 3B**). Interestingly, when comparing UBE2D3 levels in tumors classified according to XBP1 or RIDD signatures (Lhomond et al., 2018), we found that UBE2D3 was significantly upregulated in X+/R- tumors (**Fig. 3C**), suggesting the IRE1/XBP1s-dependent regulation of UBE2D3 in GBM cells. We also demonstrated the opposite roles of XBP1s and RIDD on UBE2D3 expression, as well as the dominant role of XBP1s in the upregulation of UBE2D3 expression using two independent GBM cohorts, namely GBMmark and TCGA (**Fig. S3A-D**).

To validate the transcriptome-based findings, we determined the UBE2D3 expression level in cells with abrogated IRE1 signaling and found a significant reduction in UBE2D3 mRNA in both U87 DN and RADH87 cells overexpressing Q780* IRE1 mutant (**Fig. 3D**). Next, we used MatInspector software (Cartharius et al., 2005) to screen the transcription factor binding site library and found multiple XBP1 binding sites within UBE2D3 promoter region (**Fig. S3E**). In addition, we scrutinized public ChIP experiments datasets and further confirmed that XBP1s binds to DNA fragments comprised within UBE2D3 promoter region (http://dbarchive.biosciencedbc.jp/kyushu-u/hg19/target/XBP1.10.html) (Chen et al., 2014). UBE2D3 expression also positively correlated with that of XBP1 in a TCGA cohort of GBM specimens (**Fig. 3E**) and GBM cell lines exposed to a time-course tunicamycin treatment (**Fig. S3F**). Lastly, we demonstrated that silencing of XBP1 in GBM cells resulted in significant reduction of UBE2D3 mRNA level **(Fig. 3F)** and this effect was rescued with XBP1s overexpression (**Fig. 3G, Fig S3G**). This indicated that XBP1s acts as a transcriptional regulator of UBE2D3 expression.

Overall, our results suggest that IRE1 contributes to the fine-tuning of UBE2D3 expression in GBM cells; it predominantly promotes the UBE2D3 upregulation by engaging the XBP1 transcription factor, while activates RIDD to reduce UBE2D3 abundance (**Fig. 3H**). To further document this and to provide additional evidence on the role of UBE2D3 in neutrophil-mediated immunity, we stratified the GBMmark cohort according to UBE2D3 mRNA level and carried out functional enrichment analysis of genes that were found differentially expressed between the tumors with high or low UBE2D3 expression, called "UBE2D3 High" and "UBE2D3 Low", respectively (see Materials & Methods). As a result, we identified a cluster of inflammatory genes that were markedly upregulated in UBE2D3 high tumors (**Fig. 3I**). Those included genes involved in cytokine secretion (GPAM, FOXP1), members of IL6

signaling pathway (such as ST18, IL6R) and molecules mediating acute inflammatory response (including TRPV1, ORM1 or FN1).

The IRE1/UBE2D3 axis controls neutrophil recruitment to GBM through the activation of NFκB

Next, to further document how UBE2D3 activity in tumor cells can promote neutrophil infiltration, we performed *in vitro* neutrophil migration assay with culture media derived from U87 cells transiently transfected with plasmid coding for UBE2D3 (**Fig. S4A).** Conditioned media from UBE2D3 overexpressing cells prompted neutrophils migration compared to media conditioned by control cells (**Fig. 4A**). Next, we transfected increasing concentrations of UBE2D3 plasmid in both U87 and RADH87 cells (**Fig. S4A-C**) and evaluated the expression of neutrophil-attracting chemokines using RT-qPCR. This showed that the expression of CXCL2, IL6 and IL8 was markedly induced upon UBE2D3 overexpression (**Fig. 4B**). This observation was also confirmed in UBE2D3 stably transfected lines (**Fig. S4D-E**). Moreover, using GBM patients' specimens, we demonstrated that tumors with high UBE2D3 expression levels also expressed significantly higher levels of CXCL2, IL6 and IL8 mRNA (**Fig. 4C**). The expression of these pro-inflammatory mediators is controlled by NFκB signaling (Kunsch and Rosen, 1993; Libermann and Baltimore, 1990). As such, overexpression of UBE2D3 led to the degradation of NFκB inhibitor, IκB and concomitant NFκB pathway activation, as manifested by increased phosphorylation of NFκB protein (**Fig. 4D**, **Fig. S4F-G,** (Wu et al., 2010)). This effect was not potentiated under tunicamycin treatment, suggesting that UBE2D3 may promote inflammation independently of ER stress. In addition, treatment of U87 cells with the NFκB inhibitor, JSH-23, which precludes the nuclear translocation of NFκB and consequently its transcriptional activity, impeded the UBE2D3-dependent increase in CXCL2, IL6 and IL8 mRNA expression (**Fig. 4E**). IRE1 kinase domain was reported to control NFκB signaling by maintaining the basal activity of IκB kinase (IKK) under ER stress (Tam et al., 2012), however, its precise role in NFκB-dependent immune response in cancer is poorly described. Therefore, based on the above findings, we hypothesized the existence of tight interplay between IRE1 and UBE2D3 pathways in the regulation of NFκB activation (**Fig. 4F**). As such, IRE1 would balance UBE2D3 expression levels in GBM through the opposite actions of XBP1s and RIDD, while UBE2D3, as an E2 of ubiquitin system would as well negatively regulate IRE1 expression (**Fig. S4H-I**). Overall, this tightly regulated signaling circuit controls NFκB-mediated chemokines synthesis and inflammatory response in GBM.

UBE2D3 cooperates with the Ubiquitin E3 ligase MIB1 to degrade IκB and trigger NFκB-pro-inflammatory response

To identify the putative E3 ligase(s) involved in the degradation of IκB and/or activation of NFκB signaling as well as to investigate the global effect of UBE2D3 on proteins ubiquitination in GBM, we next carried out the label-free quantitative MS/MS analysis using cells with stable overexpression of UBE2D3 (**Fig. 5A**). Total proteins were extracted from RADH87 control and RADH87_UBE2D3 cells treated or not with the ER stress inducer, tunicamycin. Precipitated proteins were then subjected to trypsin digestion, followed or not by purification of ubiquitin-derived diglycine (di-Gly) remnants and concomitant MS/MS analysis of both total and ubiquitinated peptides (**Fig. 5B**). Among significantly up- and downregulated proteins in UBE2D3 overexpressing cells compared to control, we identified a set of proteins involved in proteostasis control as well as in the inflammatory response (**Fig. 5C**). Furthermore, we found a tight interaction between those ER-related entities that mainly function in protein metabolic processes (**Fig. 5D**) and showed an enriched association with extracellular vesicles (**Fig. S5**), highlighting a key role of UBE2D3 in the ER protein turnover and secretion.

We next analyzed peptides containing the di-Gly ubiquitin remnants for each analyzed sample (**Fig. S5B-C**) and compared the differentially ubiquitinated proteins between the most extreme conditions, namely RADH87 control (EV) cells cultivated without stress and RADH87_UBE2D3 cells treated with tunicamycin, reasoning that this approach would encompass the effect of UBE2D3 on protein ubiquitination in both basal and ER stress conditions (**Fig. 5E**). We identified forty-five proteins, whose ubiquitination was significantly altered in the context of UBE2D3 overexpression and ER stress in GBM (**Fig. 5F**). Interestingly, when intersecting the list of those significantly up- and downregulated ubiquitinated proteins, we found that only one of the enriched molecules was shared between groups (**Fig. S5D**), suggesting that UBE2D3 engaged distinct machineries to exert its E2 functions in response to ER stress or in basal ER physiology. Functional enrichment analysis further revealed that UBE2D3 was mainly mediating the ubiquitination of proteins involved in cellular response to environmental stresses, while it abrogates the ubiquitin/proteasome system-dependent degradation of proteins associated with ER-to-Golgi transport (**Fig. 5G**), which further supports our findings on the role of UBE2D3 in the regulation of ER homeostasis and secretory pathway. Within the proteins purified from UBE2D3 overexpressing cells that showed divergent ubiquitination patterns compared to parental cells, we have identified the E3 ligase MIB1. We thus focused our attention on that molecule since MIB1 was reported to participate in the control of NFκB activation (Liu et al., 2012) and also to interact with UBE2D3 E2 enzyme (van Wijk et al., 2009). Therefore, we next investigated whether MIB1 might cooperate with UBE2D3 to trigger the degradation of IκB, leading to the activation of NFκB signaling and subsequent synthesis of neutrophil-attracting chemokines in GBM. We targeted MIB1 expression using specific siRNA in control and UBE2D3 overexpressing cells (**Fig. S5E**)

and investigated its effect on NFκB pathway activation. We found that MIB1 silencing partially prevented the UBE2D3-mediated degradation of IκB protein (**Fig. 5H**) and subsequently the upregulation of pro-inflammatory chemokines IL6 and IL8 in UBE2D3 overexpressing cells compared to control counterparts (**Fig. 5I**). Overall, these results suggest the existence of a signaling axis involving IRE1, UBE2D3 and MIB1 sufficient to trigger the activation of NFκB-dependent pro-inflammatory response in GBM.

UBE2D3 controls pro-tumoral inflammation *in vivo* and increases GBM cell aggressiveness

To further validate the importance of the IRE1/UBE2D3 signaling axis in GBM, we used a GBM syngeneic mouse model that allowed us to investigate the impact of UBE2D3 on neutrophil infiltration to GBM *in vivo*. To this end, GL261 control and UBE2D3 overexpressing cells (denoted as GL261_UBE2D3 hereafter, **Fig. S6A**) were injected into the brain of immunocompetent C57BL/6 mice. Twenty-four days post-injections tumors were resected and subjected to the immunohistochemical analysis for quantifying the immune infiltrate. Interestingly, GL261_UBE2D3 cells produced larger tumors when compared to the control counterparts (**Fig. 6A**), which was not attributed to the intrinsic characteristics of the cells, since both lines showed similar proliferation rate *in vitro* (**Fig. S6B**). This suggests that the growth advantage of UBE2D3 overexpressing tumors might emerge from the interaction with stroma and/or tumor microenvironment. In line with this observation, GL261_UBE2D3 tumors recruited significantly higher numbers of neutrophils to GBM tissue (**Fig. 6B**) and showed an elevated induction of NFκB expression (**Fig. 6C**), which confirmed our *in vitro* findings. Since NFκB is a master regulator of inflammatory response, we tested whether UBE2D3 specifically controlled neutrophils migration to GBM or whether this mechanism would also trigger the infiltration of other immune cells. We thus quantified macrophages/microglial cells recruited *in vivo* to the control and UBE2D3 overexpressing tumors and found a significantly higher number of IBA1-positive cells (markers of macrophages/microglia) in tumors derived from GL261_UBE2D3 cells (**Fig. 6D**). Furthermore, using transcriptome data of two independent GBM cohorts, GBMmark and TCGA_GBMLGG, we also demonstrated a strong correlation between UBE2D3 expression levels and the expression of a large number of pro-inflammatory cyto/chemokines (**Fig. 6E**, **Fig. S6C**). Intriguingly, high UBE2D3 expression was also associated with increased monocytes, T cells and M2-polarized macrophages infiltration, as determined by the expression levels of their specific surface receptors (**Fig. 6F**, **Fig. S6D**). Next, to evaluate a clinical and prognostic relevance of UBE2D3 in GBM, we investigated UBE2D3 expression in brain malignancies and showed that UBE2D3 is markedly increased in GBM specimens compared to low-grade gliomas. We then compared the survival rates of

patients whose tumors were characterized by high or low UBE2D3 expression and consequently found that higher expression of UBE2D3 is of poorer prognosis (**Fig. 6G**). Lastly, we showed that temozolomide treatment had significantly less prominent effect on GL261_UBE2D3 cell death (**Fig. S6E**), which suggests that UBE2D3 might render GBM cells more resistant to chemotherapy. Taken together, our findings unveil a novel IRE1-dependent mechanism promoting pro-tumoral inflammation, which integrates the UPR signaling and ubiquitin system. Here, we demonstrated the existence of IRE1/UBE2D3 axis controlling the composition of GBM secretome through the activation of NFκB signaling (**Fig. 6H**).

DISCUSSION

Despite many advances in cancer research and the development of novel promising therapies, GBM remains incurable with poor prognosis. Given the systematic failure of the current therapeutic scheme, which involves maximal safe resection, followed by concomitant radiotherapy and chemotherapy (Stupp et al., 2005), there is an urgent need to better characterize the mechanisms underlying GBM development and progression, in order to identify novel therapeutic targets and design targeted innovative therapeutic approaches.

In the past years, we have characterized the significant relevance of UPR signaling, in particular IRE1 in GBM biology (Auf et al., 2010; Dejeans et al., 2012) and recently found that the characteristics of IRE1 signaling represented a predictive factor for GBM aggressiveness (Lhomond et al., 2018). As such, modulating ER stress signaling pathways poses an attractive therapeutic avenue for GBM treatment aiming at either increasing ER stress to levels that trigger apoptosis or decreasing the adaptive UPR machinery, leading to loss of cellular selective advantages or increased sensitivity to treatments, and subsequent death (Obacz et al., 2017a). In addition to intrinsic aggressiveness of the GBM cells, the brain tumor microenvironment, that contains among others endothelial and immune cells, is emerging as a crucial regulator of brain cancers progression (Obacz et al., 2017a; Quail and Joyce, 2017). The most abundant immune cells in GBM microenvironment are tumor-associated macrophages and microglial cells that might reach up to 30% of the tumor mass and have been often linked to disease aggressiveness (Bingle et al., 2002; Hambardzumyan et al., 2016; Wei et al., 2013); however, brain tumors are also infiltrated by other immune cells such as myeloid dendritic cells (DCs), plasmacytoid DCs, T cells and neutrophils (Quail and Joyce, 2017).

In the present work, we demonstrated that IRE1 signaling in tumor cells plays a key role in the regulation of GBM microenvironment, by promoting the recruitment of myeloid cells to the tumors. We previously found that IRE1 signaling was involved in the recruitment of macrophages and microglial cells to the tumors (Lhomond et al., 2018) and that IRE1 controlled the expression of pro-inflammatory chemokines (Logue et al., 2018; Pluquet et al., 2013). Herein, we showed that pharmacological inhibition of IRE1 signaling decreased the extend of neutrophils infiltration to GBM *in vivo*, which might be of clinical importance since elevated neutrophils recruitment correlated with poor outcome of GBM patients (**Fig. 1**). We also found that IRE1 activation in tumor cells correlated with higher expression of neutrophil-attracting chemokines (**Fig. 2**). In an attempt to identify the IRE1-downstream signaling responsible for this phenomenon, we showed that IRE1 tightly controlled the expression of UBE2D3 in GBM cells either positively by engaging the activation of XBP1s or negatively through RIDD (**Fig. 3**). Then, we found that activation of the IRE1/UBE2D3 signaling axis was in part responsible for neutrophil chemoattraction through the activation of pro-inflammatory

NFκB (**Fig. 4**). UBE2D3 is a ubiquitin-conjugating enzyme (E2) that together with ubiquitin-activating enzyme (E1) and ubiquitin ligase (E3) mediates the attachment of ubiquitin moieties to target proteins. This post-translational modification impacts on a broad range of biological processes, including protein quality control and trafficking, differentiation, cell division, signal transduction as well as inflammation (Glickman and Ciechanover, 2002; Mukhopadhyay and Riezman, 2007). UBE2D3 has been shown to control proteasomal degradation of among others p53 (Saville et al., 2004), cyclin D1 (Hattori et al., 2007), p12 subunit of DNA polymerase δ (Zhang et al., 2013) and IκBα (Wu et al., 2010). It was also reported to mediate the ubiquitination of RIG-I, event required for its activation upon viral infection initiating the type I interferon (IFN)- dependent innate immune response (Shi et al., 2017). In this work, we further demonstrated a crucial role of UBE2D3 in the regulation of immunity/inflammation in pathological conditions, such as cancer. We found that UBE2D3 is overexpressed in GBM compared to low-grade gliomas and that its elevated expression correlated with high abundance of pro-inflammatory molecules. We delineated a novel IRE1-dependent mechanism towards NFκB activation, which involves upregulation of UBE2D3 leading to the degradation of IκB through at least partially the activity of E3 ubiquitin ligase MIB1 (**Fig. 5**), the subsequent nuclear translocation of NFκB and activation of its downstream signaling (**Fig. 4**). Hence, IRE1 controls the synthesis of pro-inflammatory chemokines, including, as demonstrated here, CXCL2, IL6 and IL8. Once secreted, they not only sustain the pro-tumoral inflammatory microenvironment but can also mobilize the recruitment of immune cells to the tumor site further promoting cancer progression. As such, we showed *in vivo* that UBE2D3 overexpressing tumors were bigger in size and were infiltrated by significantly higher numbers of immune cells, such as neutrophils and macrophages/microglia (**Fig. 6**). However, our findings indicate that the aforementioned mechanism might be applicable to the infiltration by a large number of lymphocytes, highlighting the importance of understanding the IRE1/UBE2D3 axis in other cancer models, particularly in 'immune hot' tumors.

Taken together, this study implies that targeting IRE1 signaling as therapeutic approach might impede glioblastoma aggressiveness by reducing tumor cell migration, invasion and angiogenesis (Auf et al., 2010; Lhomond et al., 2018), but also by neutralizing the pro-tumoral inflammation and immunity.

MATERIALS AND METHODS

Patient samples and data – GBMmark cohort has been generated as previously described (Lhomond et al., 2018). Briefly, tumors were either clinically and genetically characterized in the department of neurosurgery of the Pellegrin Hospital (Bordeaux, France) or were obtained from the processing of biological samples through the Centre de Ressources Biologiques (CRB) Santé of Rennes BB-0033-00056. The research protocol was conducted under French legal guidelines and fulfilled the requirements of the local institutional ethics committee. The quantification procedure of mRNA abundance is described in the "Microarray data analysis" section. Messenger RNA expression data were also assessed from the publicly available GBM dataset of The Cancer Genome Atlas (TCGA) (Consortium et al., 2007; consortium, 2008) from the NCBI website platform https://gdc-portal.nci.nih.gov/ and from the TCGA-GBMLGG dataset obtained from GlioVis online tool (http://gliovis.bioinfo.cnio.es/).

Immunohistochemistry (IHC) – GBM samples were obtained from CRB Santé of Rennes BB-0033-00056. Tumor tissues were fixed in 10% neutral buffered formalin, embedded in paraffin, cut into 4-µm thick sections, mounted on slides, deparaffinized in xylene and rehydrated into PBS through a graded ethanol series. Endogenous peroxidase activity was quenched in 3% hydrogen peroxide (Roche) in PBS for 15 minutes. The IHC labeling were carried out using the H2P2 imaging platform of the faculty of Rennes. For human neutrophils immunodetection, the sections were incubated with anti-CD66b antibody (BD Biosciences), and analyzed with NIS-Elements Advanced Research Software (Nikon).

Cell culture and treatments – The U87, U87 IRE1.NCK DN cells (referred to as U87 DN) (Drogat 2007), U251 and GL261 cell lines (all from ATCC) were grown in Dulbecco's modified Eagle's medium (DMED) (Invitrogen) supplemented with 10% foetal bovine serum (FBS) (Lonza) in a 5% CO_2 humidified atmosphere at 37°C. Primary GBM cell lines were generated as previously described (Avril et al., 2012; Lhomond et al., 2018). For certain tumors, the two types of cultures have been established, adherent cell lines (RADH) grown in DMEM supplemented with 10% FCS and neurospheres (RNS, enriched in cancer stem cells) grown in DMEM/Ham's F12 GlutaMAX (Life Technologies) supplemented with B27 and N2 additives (Invitrogen, Cergy Pontoise, France), EGF (20 ng/ml) and FGF2 (20 ng/ml) (Peprotech, Tebu-Bio).

To induce ER stress, cells were treated with 5 µg/mL Tunicamycin (Tun) (Calbiochem) for the indicated time periods. For NFκB pathway inhibition, 5µM JSH-23 (Sigma) was used for 16 hours.

Antibodies and other reagents – The following primary antibodies were used: rabbit polyclonal anti-IRE1 (Santa Cruz), mouse monoclonal anti-XBP1s (Bio Legend), mouse monoclonal anti-KDEL (Enzo), mouse monoclonal anti-UBE2D3 (Abcam), rabbit monoclonal

anti-NFκB p65 (Cell Signaling), rabbit monoclonal anti-phospho-NFκB p65 (Cell Signaling), rabbit polyclonal anti-IκB (Cell Signaling), rabbit monoclonal anti-phospho-IκB (Cell Signaling), rabbit monoclonal anti-actin (Sigma), mouse monoclonal anti-tubulin (Sigma) and mouse monoclonal anti-p97 (BD Transduction Laboratories). The secondary antibodies were horseradish peroxidase (HRP) conjugated polyclonal goat anti-rabbit IgG, HRP-conjugated polyclonal goat anti-mouse IgG and HRP-conjugated polyclonal rabbit anti-goat IgG (all Dako). For transient overexpression or silencing, cells were transfected using Lipofectamine 2000 or Lipofectamine LTX (Thermo Fisher Scientific) for plasmids and Lipofectamine RNAiMAX Transfection Reagent (Thermo Fisher Scientific) for siRNA, according to the manual.

Semi-quantitative PCR and Quantitative real-time PCR (qPCR) **–** Total RNA was extracted using the Trizol reagent (Invitrogen). All RNAs were reverse transcribed with Maxima Reverse Transcriptase (Thermo Scientific), according to manufacturer protocol. All PCR reactions were performed with a MJ Mini thermal cycler from Biorad (Hercules) and qPCR with a QuantStudio™ 5 Real-Time PCR Systems from Thermo Fisher Scientific and the PowerUp™ SYBR Green Master Mix (Thermo Fisher Scientific). Experiments were performed with at least triplicates for each data point. Each sample was normalized on the basis of its expression of the GAPDH or actin gene using $2^{\Delta\Delta CT}$-method. The primers pairs used for this study are listed in **Table S1**.

Neutrophil chemoattraction assay – Neutrophils were isolated from peripheral blood of healthy donors using MACSXPRESS Neutrophil Isolation Kit (Miltenyi Biotec), according to manufacturer protocol. Neutrophils were then washed in DMEM and placed in 3 µm Boyden chambers (Merck Millipore, France), at the concentration of 0.5 x 10^6 cells/chamber in 200 µl DMEM. Chambers were simultaneously placed in 500 µl of either control DMEM or tumor conditioned media as indicated, and incubated for 2 hrs at 37°C. The migrated neutrophils (under the Boyden chambers) were collected, washed in PBS and analyzed by flow cytometry using a Novocyte flow cytometer (Acea Biosciences). The population of interest was gated according to its FSC/SSC criteria. The relative number of migrated cells was estimated by flow cytometry by counting the number of cells per microliter.

FACS analyses **–** GBM specimens were dissociated using the gentle MACS dissociator (Miltenyi Biotec) according to manufacturer's recommendations and cells were directly used for flow cytometry analysis. Cells were washed in PBS supplemented with 2% FBS and incubated with saturating concentrations of human immunoglobulins and fluorescent-labelled primary antibodies as indicated for 30 minutes at 4°C. Cells were then washed with PBS 2% FBS and analyzed by flow cytometry using a FACSCanto and Novocyte flow cytometer (BD Biosciences and Acea Biosciences). The population of interest was gated according to its FSC/SSC criteria. The dead cell population was excluded using 7AAD staining (BD

Biosciences). Data were analyzed with the FACSDiva (BD Biosciences). GBM specimens with more than 2% stained cells of total viable cells were considered positive for the immune marker of interest.

Mass spectrometry – RADH87 parental and RADH87_UBE2D3 cells were lysed with lysis buffer composed of 20 mM Tris pH 8, 1.5 mM EDTA, 150 mM NaCl, 1% Triton X-100, 0.1% SDS, 15µM MG132, 10mM NEM (N-ethylmaleimide), 10µM deubiquitinating enzymes inhibitors (DUBi, PR-619), supplemented with proteases and phosphatases inhibitor cocktails (Roche). Total proteins were precipitated overnight with 80% ice-cold acetone. Protein pellets were then washed 3 times with 80% acetone, followed by centrifugation at 500 rpm for 30 mins at 4°C. Samples were alkylated and digested with trypsin at 37°C overnight and ubiquitinated peptides were enriched with PTMScan Ubiquitin Remnant Motif (K-ε-GG) Kit (Cell Signaling Technology). After Sep Pak desalting, peptides were analyzed using an Ultimate 3000 nano-RSLC (Thermo Fisher Scientific) coupled in line with an Orbitrap ELITE (Thermo Scientific). Each sample was analyzed in triplicate. Briefly, peptides were separated on a C18 nano-column with a linear gradient of acetonitrile and analyzed in a Top 20 CID (Collision-induced dissociation) data-dependent mass spectrometry. Data were processed by database searching against Human Uniprot Proteome database using Proteome Discoverer 2.2 software (Thermo Fisher Scientific). Precursor and fragment mass tolerance were set at 7 ppm and 0.6 Da respectively. Trypsin was set as enzyme, and up to 2 missed cleavages were allowed. Oxidation (M, +15.995), GG (K, +114.043) were set as variable modification and Carbamidomethylation (C) as fixed modification. Proteins were filtered with False Discovery Rate <1% (high confidence). Lastly, quantitative values were obtained from Extracted Ion Chromatogram (XIC) and p-values were determined by ANOVA with Precursor Ions Quantifier node in Proteome Discoverer.

Syngeneic mouse model and inflammation – Eight-weeks old male C57BL/6 mice were housed in an animal care unit authorized by the French Ministries of Agriculture and Research (Biosit, Rennes, France - Agreement No. B35-238-40). The protocol used was as previously described (Auf et al., 2010). Cell implantations were at 2 mm lateral to the bregma and 3 mm in depth using GL261 (control) or GL261_UBE2D3 cells. Mice were daily clinically monitored and sacrificed twenty-four days post injection. Mouse brains were collected, fixed in 4% formaldehyde solution and paraffin embedded for histological analysis using anti-vimentin antibody (Interchim) to visualize the tumor masses. Tumor volume was then estimated by measuring the length (L) and width (W) of each tumor and was calculated using the following formula ($L \times W^2 \times 0.5$). Immune cells infiltration was monitored by immunohistochemistry using rat anti-mouse Ly6G antibody (BD Biosciences) for neutrophils, anti-IBA1 (Wako) for macrophages/microglia, while NFκB level was determined with rabbit monoclonal anti-NFκB

p65 antibody (Cell Signaling). Imaging was carried out using a Axioplan 2 epifluorescent microscope (Zeiss) equipped with a digital camera Axiocam (Zeiss).

Microarray data analysis - Complete gene expression analysis of the GBMmark microarray Agilent dataset (GEO) was performed with R (R version 3.5.0)/Bioconductor software (Huber et al., 2015). Firstly, the raw data obtained from the public repository ArrayExpress (E-MTAB-6326) (Kolesnikov et al., 2015) were pre-processed (background correction and quantile normalization) using the limma R package (Ritchie et al., 2015). Next, non-expressed probesets in the majority of the samples (that is, probesets expressed in less than 10% of the total number of patients) were filtered out, in order to remove consistently non-expressed genes. Finally, the global expression alteration patterns between "UBE2D3 High" and "UBE2D3 Low" tumors were identified. The samples were initially separated in two distinct groups, based on their relative median expression value of UBE2D3 and then, differential expression analysis was performed using the moderated t-test (from limma R package). This kind of analysis revealed 1047 Differentially expressed (DE) genes with an absolute value of log2 fold change greater than 1 and an adjusted p-value less than 0.05 (FDR).
To shed light on the molecular mechanisms involved in the IRE1-UBE2D3 signaling axis, the aforementioned list of DE genes, was used as an input to the BioInfoMiner interpretation web platform (Koutsandreas et al., 2016; Lhomond et al., 2018), which performs automated, network analysis of functional terms, integrating semantic information from different biomedical ontologies and controlled vocabularies such as Gene Ontology (GO), Reactome, Human Phenotype Ontology (HPO) and many others

Statistical analyses – Graphs and statistical analyses were performed using GraphPad Prism 7.0 software (GraphPad Software). Data are presented as mean ± SD or SEM of at least three independent experiments. Statistical significance ($p<0.05$ or less) was determined using a paired or unpaired t-test or ANOVA as appropriate, while comparison of survival curves was done using log-rank (Mantel-Cox) test. Significant variations were represented by asterisks above the corresponding bar when comparing the test with the control condition or above the line when comparing the two indicated conditions.

All other methods can be found in Supplemental Material.

Acknowledgements

This work was funded by grants from INSERM, Institut National du Cancer (INCa), Région Bretagne, Rennes Métropole, Fondation pour la recherche Médicale (FRM ; équipe labellisée 2018), EU H2020 MSCA ITN-675448 (TRAINERS), la Ligue Contre le Cancer Comités d'Ille-et-Vilaine, des Côtes d'Armor et du Morbihan and MSCA RISE-734749 (INSPIRED) to EC; PROMISE, 12CHN 204 Bilateral Greece-China Research Program of the Hellenic General Secretariat of Research and Technology and the Chinese Ministry of Research and Technology sponsored by the Program "Competitiveness and Entrepreneurship," Priority Health of the Peripheral Entrepreneurial Program of Attiki to AC. JO was supported by a post-doctoral fellowship from Région Bretagne.

REFERENCES

Almanza, A., Carlesso, A., Chintha, C., Creedican, S., Doultsinos, D., Leuzzi, B., Luis, A., McCarthy, N., Montibeller, L., More, S.*, et al.* (2018). Endoplasmic reticulum stress signalling - from basic mechanisms to clinical applications. FEBS J.

Auf, G., Jabouille, A., Guerit, S., Pineau, R., Delugin, M., Bouchecareilh, M., Magnin, N., Favereaux, A., Maitre, M., Gaiser, T.*, et al.* (2010). Inositol-requiring enzyme 1alpha is a key regulator of angiogenesis and invasion in malignant glioma. Proc Natl Acad Sci U S A *107*, 15553-15558.

Avril, T., Vauleon, E., Hamlat, A., Saikali, S., Etcheverry, A., Delmas, C., Diabira, S., Mosser, J., and Quillien, V. (2012). Human glioblastoma stem-like cells are more sensitive to allogeneic NK and T cell-mediated killing compared with serum-cultured glioblastoma cells. Brain Pathol *22*, 159-174.

Badie, B., and Schartner, J.M. (2000). Flow cytometric characterization of tumor-associated macrophages in experimental gliomas. Neurosurgery *46*, 957-961; discussion 961-952.

Bingle, L., Brown, N.J., and Lewis, C.E. (2002). The role of tumour-associated macrophages in tumour progression: implications for new anticancer therapies. J Pathol *196*, 254-265.

Bowman, R.L., Wang, Q., Carro, A., Verhaak, R.G., and Squatrito, M. (2017). GlioVis data portal for visualization and analysis of brain tumor expression datasets. Neuro Oncol *19*, 139-141.

Calfon, M., Zeng, H., Urano, F., Till, J.H., Hubbard, S.R., Harding, H.P., Clark, S.G., and Ron, D. (2002). IRE1 couples endoplasmic reticulum load to secretory capacity by processing the XBP-1 mRNA. Nature *415*, 92-96.

Cartharius, K., Frech, K., Grote, K., Klocke, B., Haltmeier, M., Klingenhoff, A., Frisch, M., Bayerlein, M., and Werner, T. (2005). MatInspector and beyond: promoter analysis based on transcription factor binding sites. Bioinformatics *21*, 2933-2942.

Chen, X., Iliopoulos, D., Zhang, Q., Tang, Q., Greenblatt, M.B., Hatziapostolou, M., Lim, E., Tam, W.L., Ni, M., Chen, Y.*, et al.* (2014). XBP1 promotes triple-negative breast cancer by controlling the HIF1alpha pathway. Nature *508*, 103-107.

Chen, Y., and Brandizzi, F. (2013). IRE1: ER stress sensor and cell fate executor. Trends Cell Biol *23*, 547-555.

Chevet, E., Hetz, C., and Samali, A. (2015). Endoplasmic reticulum stress-activated cell reprogramming in oncogenesis. Cancer Discov *5*, 586-597.

Consortium, E.P., Birney, E., Stamatoyannopoulos, J.A., Dutta, A., Guigó, R., Gingeras, T.R., Margulies, E.H., Weng, Z., Snyder, M., Dermitzakis, E.T.*, et al.* (2007). Identification and analysis of functional elements in 1% of the human genome by the ENCODE pilot project. Nature *447*, 799-816.

consortium, T. (2008). Comprehensive genomic characterization defines human glioblastoma genes and core pathways. Nature *455*, 1061-1068.

Dejeans, N., Pluquet, O., Lhomond, S., Grise, F., Bouchecareilh, M., Juin, A., Meynard-Cadars, M., Bidaud-Meynard, A., Gentil, C., Moreau, V.*, et al.* (2012). Autocrine control of glioma cells adhesion and migration through IRE1alpha-mediated cleavage of SPARC mRNA. J Cell Sci *125*, 4278-4287.

Dufey, E., Sepulveda, D., Rojas-Rivera, D., and Hetz, C. (2014). Cellular mechanisms of endoplasmic reticulum stress signaling in health and disease. 1. An overview. Am J Physiol Cell Physiol *307*, C582-594.

Glickman, M.H., and Ciechanover, A. (2002). The ubiquitin-proteasome proteolytic pathway: destruction for the sake of construction. Physiol Rev *82*, 373-428.

Grootjans, J., Kaser, A., Kaufman, R.J., and Blumberg, R.S. (2016). The unfolded protein response in immunity and inflammation. Nat Rev Immunol *16*, 469-484.
Gu, Z., Eils, R., and Schlesner, M. (2016). Complex heatmaps reveal patterns and correlations in multidimensional genomic data. Bioinformatics *32*, 2847-2849.
Hambardzumyan, D., Gutmann, D.H., and Kettenmann, H. (2016). The role of microglia and macrophages in glioma maintenance and progression. Nat Neurosci *19*, 20-27.
Han, D., Lerner, A.G., Vande Walle, L., Upton, J.P., Xu, W., Hagen, A., Backes, B.J., Oakes, S.A., and Papa, F.R. (2009). IRE1alpha kinase activation modes control alternate endoribonuclease outputs to determine divergent cell fates. Cell *138*, 562-575.
Hattori, H., Zhang, X., Jia, Y., Subramanian, K.K., Jo, H., Loison, F., Newburger, P.E., and Luo, H.R. (2007). RNAi screen identifies UBE2D3 as a mediator of all-trans retinoic acid-induced cell growth arrest in human acute promyelocytic NB4 cells. Blood *110*, 640-650.
Hetz, C., Martinon, F., Rodriguez, D., and Glimcher, L.H. (2011). The unfolded protein response: integrating stress signals through the stress sensor IRE1alpha. Physiol Rev *91*, 1219-1243.
Hollien, J., and Weissman, J.S. (2006). Decay of endoplasmic reticulum-localized mRNAs during the unfolded protein response. Science *313*, 104-107.
Hu, P., Han, Z., Couvillon, A.D., Kaufman, R.J., and Exton, J.H. (2006). Autocrine tumor necrosis factor alpha links endoplasmic reticulum stress to the membrane death receptor pathway through IRE1alpha-mediated NF-kappaB activation and down-regulation of TRAF2 expression. Mol Cell Biol *26*, 3071-3084.
Huber, W., Carey, V.J., Gentleman, R., Anders, S., Carlson, M., Carvalho, B.S., Bravo, H.C., Davis, S., Gatto, L., Girke, T.*, et al.* (2015). Orchestrating high-throughput genomic analysis with Bioconductor. Nat Methods *12*, 115-121.
Kim, S., Joe, Y., Kim, H.J., Kim, Y.S., Jeong, S.O., Pae, H.O., Ryter, S.W., Surh, Y.J., and Chung, H.T. (2015). Endoplasmic reticulum stress-induced IRE1alpha activation mediates cross-talk of GSK-3beta and XBP-1 to regulate inflammatory cytokine production. J Immunol *194*, 4498-4506.
Kolesnikov, N., Hastings, E., Keays, M., Melnichuk, O., Tang, Y.A., Williams, E., Dylag, M., Kurbatova, N., Brandizi, M., Burdett, T.*, et al.* (2015). ArrayExpress update--simplifying data submissions. Nucleic Acids Res *43*, D1113-1116.
Koutsandreas, T., Binenbaum, I., Pilalis, E., Valavanis, I., Papadodima, O., and Chatziioannou, A. (2016). Analyzing and Visualizing Genomic Complexity for the Derivation of the Emergent Molecular Networks. Int. J. Monit. Surveill. Technol. Res. *4*, 30-49.
Kunsch, C., and Rosen, C.A. (1993). NF-kappa B subunit-specific regulation of the interleukin-8 promoter. Mol Cell Biol *13*, 6137-6146.
Le Reste, P.J., Avril, T., Quillien, V., Morandi, X., and Chevet, E. (2016). Signaling the Unfolded Protein Response in primary brain cancers. Brain Res *1642*, 59-69.
Lhomond, S., Avril, T., Dejeans, N., Voutetakis, K., Doultsinos, D., McMahon, M., Pineau, R., Obacz, J., Papadodima, O., Jouan, F.*, et al.* (2018). Dual IRE1 RNase functions dictate glioblastoma development. EMBO Mol Med *10*.
Libermann, T.A., and Baltimore, D. (1990). Activation of interleukin-6 gene expression through the NF-kappa B transcription factor. Mol Cell Biol *10*, 2327-2334.
Liu, L.J., Liu, T.T., Ran, Y., Li, Y., Zhang, X.D., Shu, H.B., and Wang, Y.Y. (2012). The E3 ubiquitin ligase MIB1 negatively regulates basal IkappaBalpha level and modulates NF-kappaB activation. Cell Res *22*, 603-606.

Logue, S.E., McGrath, E.P., Cleary, P., Greene, S., Mnich, K., Almanza, A., Chevet, E., Dwyer, R.M., Oommen, A., Legembre, P.*, et al.* (2018). Inhibition of IRE1 RNase activity modulates the tumor cell secretome and enhances response to chemotherapy. Nat Commun *9*, 3267.

Martinon, F., Chen, X., Lee, A.H., and Glimcher, L.H. (2010). TLR activation of the transcription factor XBP1 regulates innate immune responses in macrophages. Nat Immunol *11*, 411-418.

Maurel, M., Chevet, E., Tavernier, J., and Gerlo, S. (2014). Getting RIDD of RNA: IRE1 in cell fate regulation. Trends Biochem Sci *39*, 245-254.

Maurel, M., McGrath, E.P., Mnich, K., Healy, S., Chevet, E., and Samali, A. (2015). Controlling the unfolded protein response-mediated life and death decisions in cancer. Semin Cancer Biol *33*, 57-66.

Mukhopadhyay, D., and Riezman, H. (2007). Proteasome-independent functions of ubiquitin in endocytosis and signaling. Science *315*, 201-205.

Obacz, J., Avril, T., Le Reste, P.J., Urra, H., Quillien, V., Hetz, C., and Chevet, E. (2017a). Endoplasmic reticulum proteostasis in glioblastoma-From molecular mechanisms to therapeutic perspectives. Sci Signal *10*.

Obacz, J., Avril, T., Rubio-Patino, C., Bossowski, J.P., Igbaria, A., Ricci, J.E., and Chevet, E. (2017b). Regulation of tumor-stroma interactions by the unfolded protein response. FEBS J.

Pluquet, O., Dejeans, N., Bouchecareilh, M., Lhomond, S., Pineau, R., Higa, A., Delugin, M., Combe, C., Loriot, S., Cubel, G.*, et al.* (2013). Posttranscriptional regulation of PER1 underlies the oncogenic function of IREalpha. Cancer Res *73*, 4732-4743.

Powell, D.R., and Huttenlocher, A. (2016). Neutrophils in the Tumor Microenvironment. Trends Immunol *37*, 41-52.

Quail, D.F., and Joyce, J.A. (2017). The Microenvironmental Landscape of Brain Tumors. Cancer Cell *31*, 326-341.

Ritchie, M.E., Phipson, B., Wu, D., Hu, Y., Law, C.W., Shi, W., and Smyth, G.K. (2015). limma powers differential expression analyses for RNA-sequencing and microarray studies. Nucleic Acids Res *43*, e47.

Saville, M.K., Sparks, A., Xirodimas, D.P., Wardrop, J., Stevenson, L.F., Bourdon, J.C., Woods, Y.L., and Lane, D.P. (2004). Regulation of p53 by the ubiquitin-conjugating enzymes UbcH5B/C in vivo. J Biol Chem *279*, 42169-42181.

Shanware, N.P., Bray, K., Eng, C.H., Wang, F., Follettie, M., Myers, J., Fantin, V.R., and Abraham, R.T. (2014). Glutamine deprivation stimulates mTOR-JNK-dependent chemokine secretion. Nat Commun *5*, 4900.

Shi, Y., Yuan, B., Zhu, W., Zhang, R., Li, L., Hao, X., Chen, S., and Hou, F. (2017). Ube2D3 and Ube2N are essential for RIG-I-mediated MAVS aggregation in antiviral innate immunity. Nat Commun *8*, 15138.

Stupp, R., Mason, W.P., van den Bent, M.J., Weller, M., Fisher, B., Taphoorn, M.J., Belanger, K., Brandes, A.A., Marosi, C., Bogdahn, U.*, et al.* (2005). Radiotherapy plus concomitant and adjuvant temozolomide for glioblastoma. N Engl J Med *352*, 987-996.

Tam, A.B., Mercado, E.L., Hoffmann, A., and Niwa, M. (2012). ER stress activates NF-kappaB by integrating functions of basal IKK activity, IRE1 and PERK. PLoS One *7*, e45078.

Urano, F., Wang, X., Bertolotti, A., Zhang, Y., Chung, P., Harding, H.P., and Ron, D. (2000). Coupling of stress in the ER to activation of JNK protein kinases by transmembrane protein kinase IRE1. Science *287*, 664-666.

Urra, H., Dufey, E., Avril, T., Chevet, E., and Hetz, C. (2016). Endoplasmic Reticulum Stress and the Hallmarks of Cancer. Trends Cancer *2*, 252-262.

van Wijk, S.J., de Vries, S.J., Kemmeren, P., Huang, A., Boelens, R., Bonvin, A.M., and Timmers, H.T. (2009). A comprehensive framework of E2-RING E3 interactions of the human ubiquitin-proteasome system. Mol Syst Biol *5*, 295.

Wei, J., Gabrusiewicz, K., and Heimberger, A. (2013). The controversial role of microglia in malignant gliomas. Clin Dev Immunol *2013*, 285246.

Wu, K., Kovacev, J., and Pan, Z.Q. (2010). Priming and extending: a UbcH5/Cdc34 E2 handoff mechanism for polyubiquitination on a SCF substrate. Mol Cell *37*, 784-796.

Zhang, S., Zhou, Y., Sarkeshik, A., Yates, J.R., 3rd, Thomson, T.M., Zhang, Z., Lee, E.Y., and Lee, M.Y. (2013). Identification of RNF8 as a ubiquitin ligase involved in targeting the p12 subunit of DNA polymerase delta for degradation in response to DNA damage. J Biol Chem *288*, 2941-2950.

FIGURE LEGEND

Figure 1. Impact of IRE1 on neutrophils recruitment to GBM *in vitro* and *in vivo*. A) Total immune infiltrate of human GBM tissues (n=65) as analyzed by flow cytometry using anti-CD45 and anti-CD11b antibodies. Number of tumors infiltrated by specific leukocytes populations are shown in circles. **B)** mRNA expression of neutrophil-specific markers, CD66b, MPO, PGLYRP1, BTNL8 and CD177 in the in-house GBM cohort (n=119). **C)** Representative photographs of neutrophils presence in GBM tissue as analyzed by immunohistochemistry with anti-CD66b antibody. **D)** Survival curve of GBM patients with high (red line, n=76) or low (blue line, n=76) neutrophils infiltration as determined according to MPO expression using GlioVis tool. Median MPO expression was used as a cut-off to select the tumors with high or low neutrophils infiltration. **E)** mRNA expression of neutrophil-marker CD177 in tumors with high (red) or low (blue) IRE1 activity as stratified in (Lhomond et al., 2018). **F-G)** Freshly isolated neutrophils were placed in Boyden chambers towards media conditioned by U87 or U87 DN (F), or by RADH87 parental cells or cells overexpressing IRE1 WT or Q780* mutant cells (G) and incubated for 2 hours. Migrating cells were then quantified by flow cytometry using FCS/SSC parameters. Data are represented as percentage of neutrophils migrated through the chamber compared to the initial number of cells placed in the insert (n=3, mean ± SD). (*): $p<0.05$, (**): $p<0.01$, (****): $p<0.0001$. **H)** Representative immunohistological analysis of neutrophils infiltration in GBM specimens resected from mice treated with empty plug or plug with IRE1 inhibitor MKC8866. Neutrophils were detected with anti-Ly6G antibody. Bar scale 100µm. **I)** Semi-quantitative analysis of Ly6G staining (marker of mouse neutrophils) in tumors from (H). At least thirty random fields from tumor tissue and at least thirty random fields from tumor periphery were quantified for control (PLUG) and MKC-treated group. (*): $p<0.05$.

Figure 2. IRE1-mediated synthesis of neutrophil-attracting chemokines. A) Heat-map representation of the correlation between neutrophils migration in Boyden chamber assay and secretion of chemokines into culture media of GBM cell lines. The color scale representation was generated using MeV tool (http://mev.tm4.org/) and corresponded to the absolute quantification of the concentration of selected chemokine (pg/ml), as determined with Bio-Plex Multiplex immunoassays. Migration pace (gray scale) corresponds to the percentage of neutrophils migrated through Boyden chamber as quantified in Fig.S3A. **B)** Correlation between CXCL2, IL6 and IL8 secretion and neutrophils migration towards GBM-conditioned media. **C)** mRNA expression of CXCL2, IL6 and IL8 in the population of tumors with high (red) or low (blue) neutrophils infiltration, as determined according to MPO or CD177 levels. Hierarchical clustering of GBM patients (GBMmark cohort) based on IRE1 activity was obtained from (Lhomond et al., 2018). **D-E)** Quantification of the expression of neutrophil-attracting chemokines using RT-qPCR in U87 and U87 DN cells (D) and RADH87 parental

cells or RADH87 cells overexpressing wild-type (WT) or Q780* IRE1 mutant (E). Data are representative of three independent experiments. (**): p<0.01, (***): p<0.001, (****): p<0.0001.

Figure 3. IRE1/XBP1-dependent regulation of UBE2D3 expression. A) mRNA expression of UBE2D3 in GBM specimens categorized according to their IRE1 activity, as in (Lhomond et al., 2018). **B)** mRNA expression of UBE2D3 in tumors with high (red) or low (blue) neutrophils infiltration, as determined by MPO levels. **C)** mRNA expression of UBE2D3 in the XBP1+/RIDD- (X+/R-; red) and XBP1-/RIDD+ (X-/R+; blue) tumors from TCGA cohort, classified as in (Lhomond et al., 2018). **D)** Quantification of UBE2D3 mRNA expression by RT-qPCR in cells with active (U87 control (par) and RADH87 parental (par)) and inactive IRE1 signaling (U87 DN and RADH87 overexpressing Q780* mutant (IRE1_Q)). **E)** Correlation between UBE2D3 and XBP1 mRNA levels in TCGA GBM cohort. TCGA_GBMLGG dataset was obtained from GlioVis (http://gliovis.bioinfo.cnio.es/). **F)** Quantitation of UBE2D3 expression using RT-qPCR in U87 cells silenced or not for XBP1. Data are representative of five independent experiments. (*): p<0.05. **G)** Quantitation of UBE2D3 expression with RT-qPCR in U87 cells and RADH87 cells overexpressing IRE1 Q780* mutant (RADH87 Q) and transfected with empty-vector (EV) or XBP1s expression plasmid. Data are representative of three independent experiments. (*): p<0.05, (***): p<0.001. **H)** Schematic representation of the antagonistic XBP1 and RIDD signals regulating UBE2D3 expression. The predominant role of XBP1 in that regulation is represented by thick black line, while secondary effect of RIDD is delignated in gray. **I)** Hierarchical clustering of mRNA expression (z_score) of immune-related genes derived from the functional enrichment analysis in GBM stratified according to UBE2D3 levels. Pearson average distance was used as similarity measure for the clustering of genes (Gu et al., 2016).

Figure 4. Impact of IRE1/UBE2D3 axis on NFκB pathway activation and chemokines synthesis. A) Migration of neutrophils isolated from blood of healthy donors in Boyden chamber assay towards media conditioned by U87 control (ctl) and UBE2D3 overexpressing cells. Data are represented as total number of neutrophils migrated through the chamber (n=3, mean ± SD). (*): p<0.05. **B)** Quantification of the expression of CXCL2, IL6 and IL8 using RT-qPCR in U87 control (EV) or UBE2D3 overexpressing cells. Data are representative of three independent experiments. (*): p<0.05, (**): p<0.01, (***): p<0.001, (****): p<0.0001 **C)** Expression analysis of CXCL2, IL6 and IL8 mRNA in the UBE2D3 high (red) and low (blue) group of tumors. **D)** Western blot analysis of NFκB, phospho-NFκB, IκB and phospoho-IκB in control (empty-vector, EV) and UBE2D3 overexpressing U87 cells under basal and ER stress conditions (Tun, tunicamycin). Actin (ACT) was used as loading control. **E)** Quantification of

the expression of CXCL2, IL6 and IL8 using RT-qPCR in U87 control (EV) or UBE2D3 overexpressing cells treated or not with 5μM NFκB pathway inhibitor, JSH-23. Data are representative of three independent experiments. (*): p<0.05, (**): p<0.01, (***): p<0.001, (****): p<0.0001. **F)** Schematic representation of the model, delineating feedforward loop between IRE1 and UBE2D3 and its impact on inflammatory response in GBM. IRE1 through both XBP1 and RIDD outputs controls UBE2D3 mRNA level, that in turn together with E3 ligase of the ubiquitin system targets IRE1 for degradation. UBE2D3 directly degrades IκB, leading to the activation of NFκB signaling and its downstream targets.

Figure 5. Impact of UBE2D3 on global proteins ubiquitination and its link to proteostasis. A) Western blot analysis of UBE2D3 expression in RADH87 parental (par) and UBE2D3 overexpressing cells. **B)** Schematic representation of the MS/MS experimental setup for the purification of ubiquitinated proteins from RADH87 control (EV) and UBE2D3 overexpressing cells. **C)** Percentage of up- and downregulated proteins related to ER proteostasis or inflammation/immune response in RADH87_UBE2D3 cells compared to RADH87 control. **D)** Representation of the ER-related protein network as identified in proteomics and list of statistically enriched GO biological processes. Indicated in colors are proteins, whose expression is modulated in UBE2D3 overexpressing cells (upregulated in red, downregulated in blue). **E)** Volcano plots of differentially ubiquitinated proteins purified from control (EV) or UBE2D3 overexpressing RADH87 cells exposed or not to ER stressor, tunicamycin (Tun). Proteins with p<0.05 and log ratio >2 or log ratio <-2 are delignated in pink and green, respectively. Dots represent purified peptides corresponding to the identified proteins. **F)** List of ubiquitinated proteins significantly upregulated (pink) or downregulated (green) in the indicated conditions. EV, control RADH87 cells; UBETun, RADH87_UBE2D3 cells treated with tunicamycin. **G)** Overrepresented (pink) and underrepresented (green) GO biological processes for the set of purified ubiquitinated proteins from RADH87_UBE2D3 cells exposed to tunicamycin (Tun) compared to RADH87 control (EV) cells. Fold enrichment values are represented as the minus base 10 log of their corresponding p values. GO-term enrichments analysis was performed using STRING database (https://string-db.org/). **H)** Western blot analysis of NFκB, phospho-NFκB, IκB and phospoho-IκB level in U87 cells overexpressing UBE2D3 and silenced or not for MIB1. Actin (ACT) was used as loading control and siGL2 as silencing control. **G)** Quantification of IL6 and IL8 mRNA expression using RT-qPCR in U87 cells overexpressing UBE2D3 and silenced or not for MIB1. siGL2 was used as silencing control. (***): p<0.001, (****): p<0.0001.

Figure 6. Impact of UBE2D3 overexpression on inflammation *in vivo*. A) Left panel: brain sections from mice injected with GL261 control (ctl) or GL261_UBE2D3 cells analyzed for vimentin expression by immunohistochemistry. Right panel: quantification of tumor volume between control (ctl) and UBE2D3 overexpressing (oe) group. **B-D)** Left panel: Representative immunohistological photographs of neutrophils infiltration (B), NFκB expression (C) or macrophages/microglia infiltration in GL261 control (ctl) or GL261_UBE2D3 tumors as detected by anti-Ly6G antibody, anti-NFκB p65 antibody or anti-IBA1 antibody, respectively. Right panel: semi-quantitative analysis of Ly6G staining (B), NFκB staining (C) or IBA1 staining (D) in GL261 control (ctl) and GL261_UBE2D3 tumors. At least forty random fields from tumor tissue and at least forty random fields from tumor periphery were quantified for control (ctl) and UBE2D3 overexpressing (oe) group. (*): $p<0.05$, (**): $p<0.01$. **E)** Correlation between UBE2D3 mRNA level and indicated cyto/chemokines expression in GBM cohort. GFAP expression (astrocyte marker) was used as negative control. **F)** Correlation between UBE2D3 mRNA level and expression of indicated immune cell-specific receptors in GBM cohort. GFAP expression (astrocyte marker) was used as negative control. **G)** Comparison of UBE2D3 expression in low-grade gliomas (LGG) and glioblastoma (GBM) and its impact on patients' survival. **H)** Schematic representation of IRE1/UBE2D3 axis in the regulation of pro-tumoral inflammation.

Figure 1

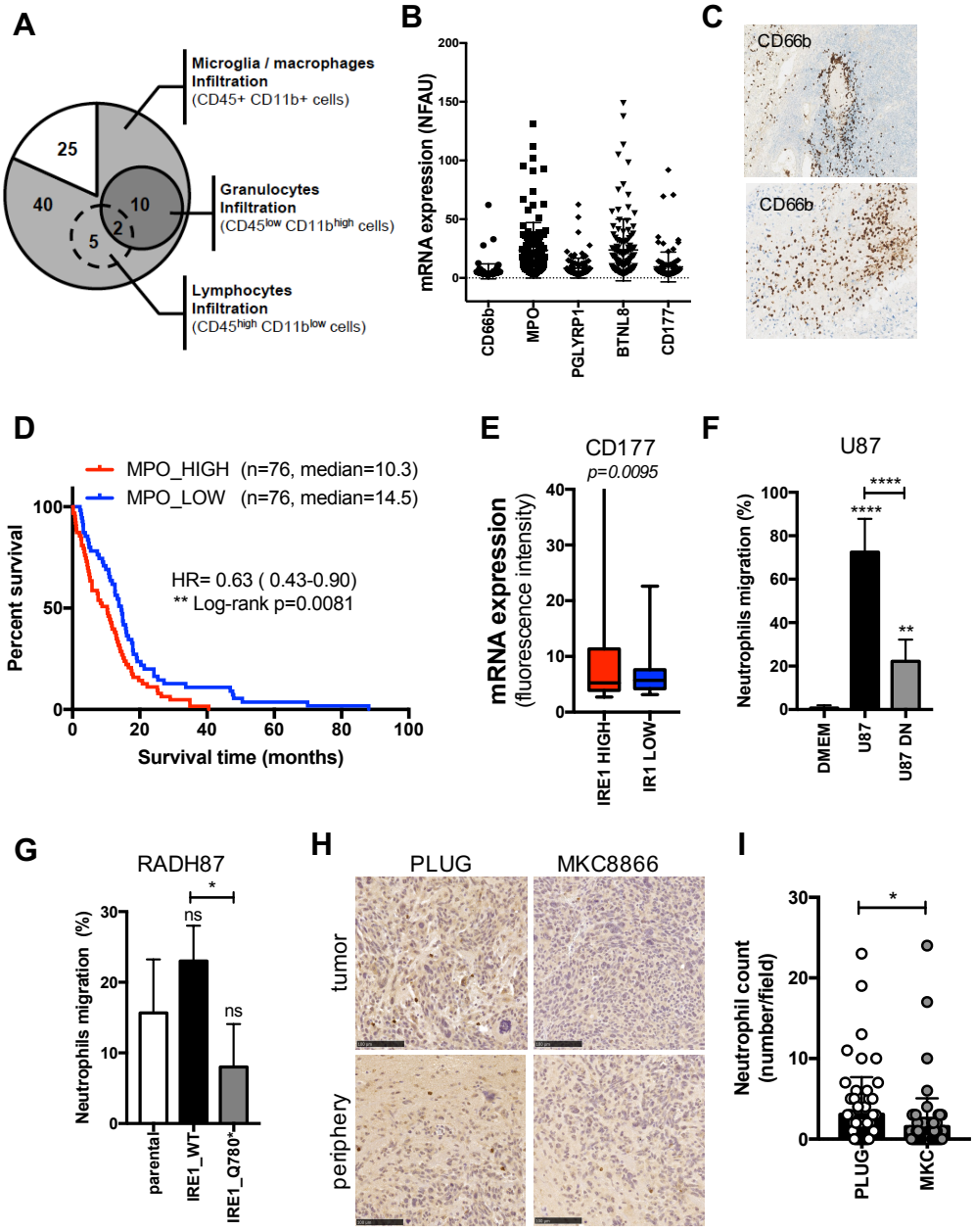

Figure 2

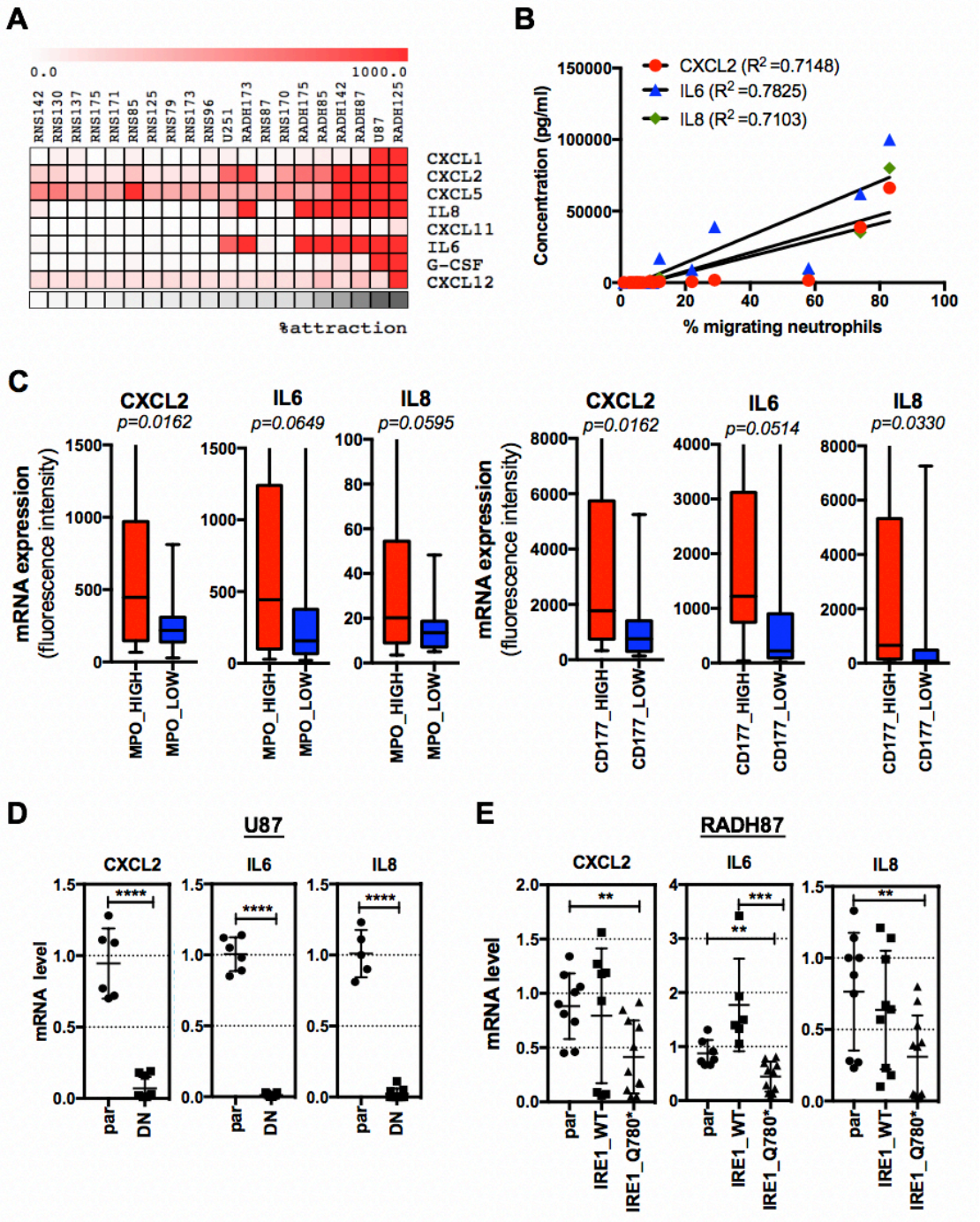

Figure 3

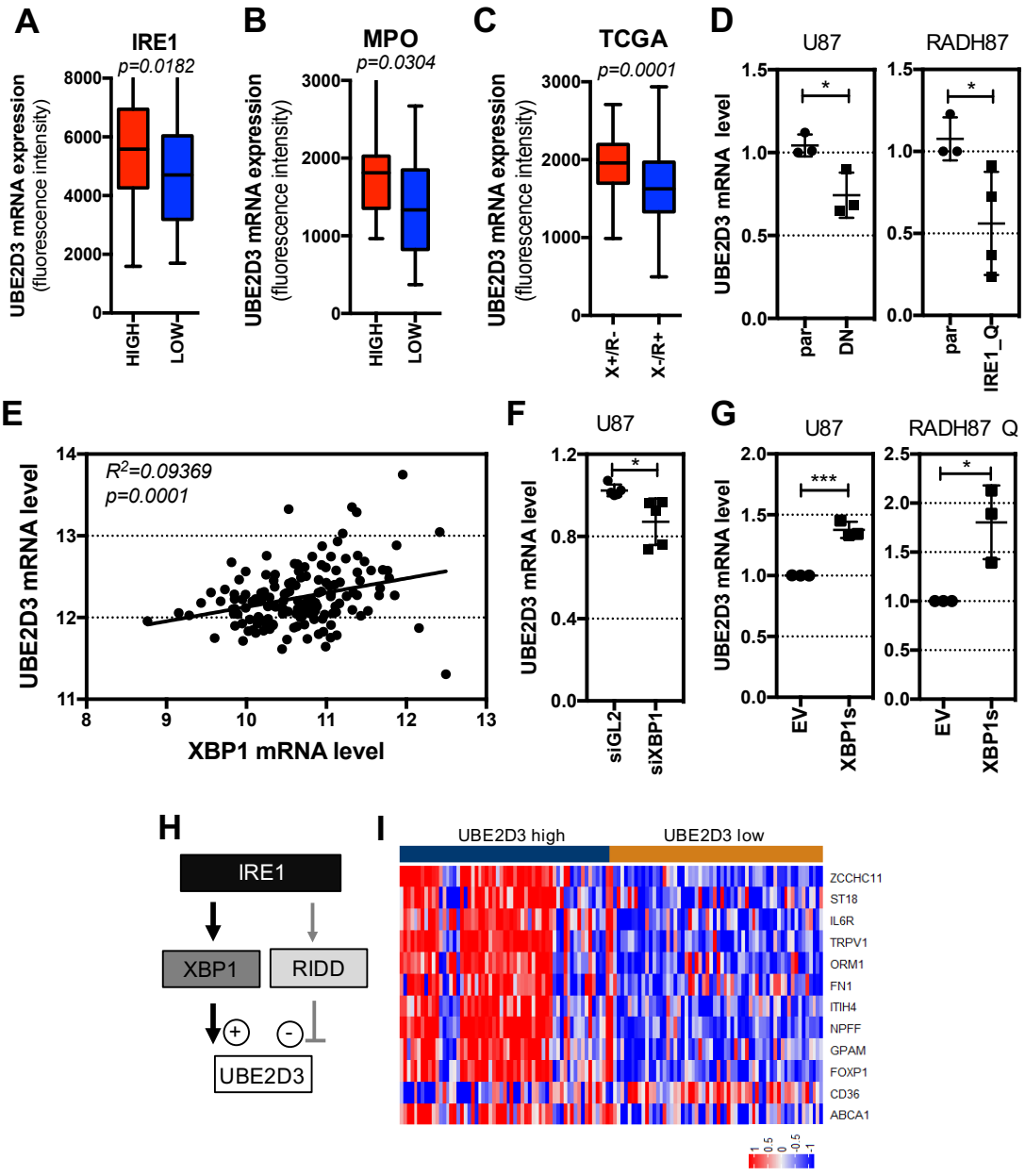

Figure 4

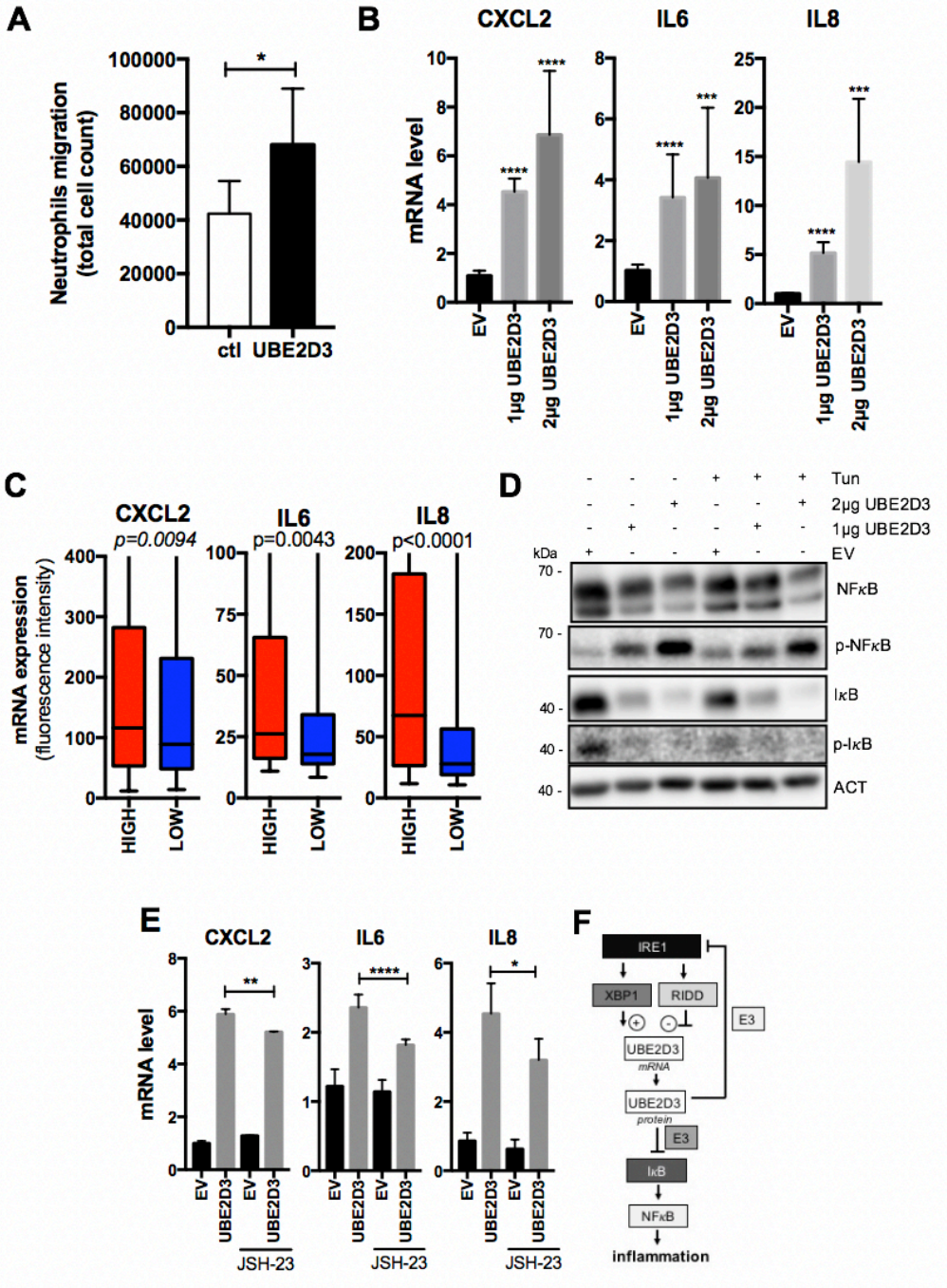

Figure 5

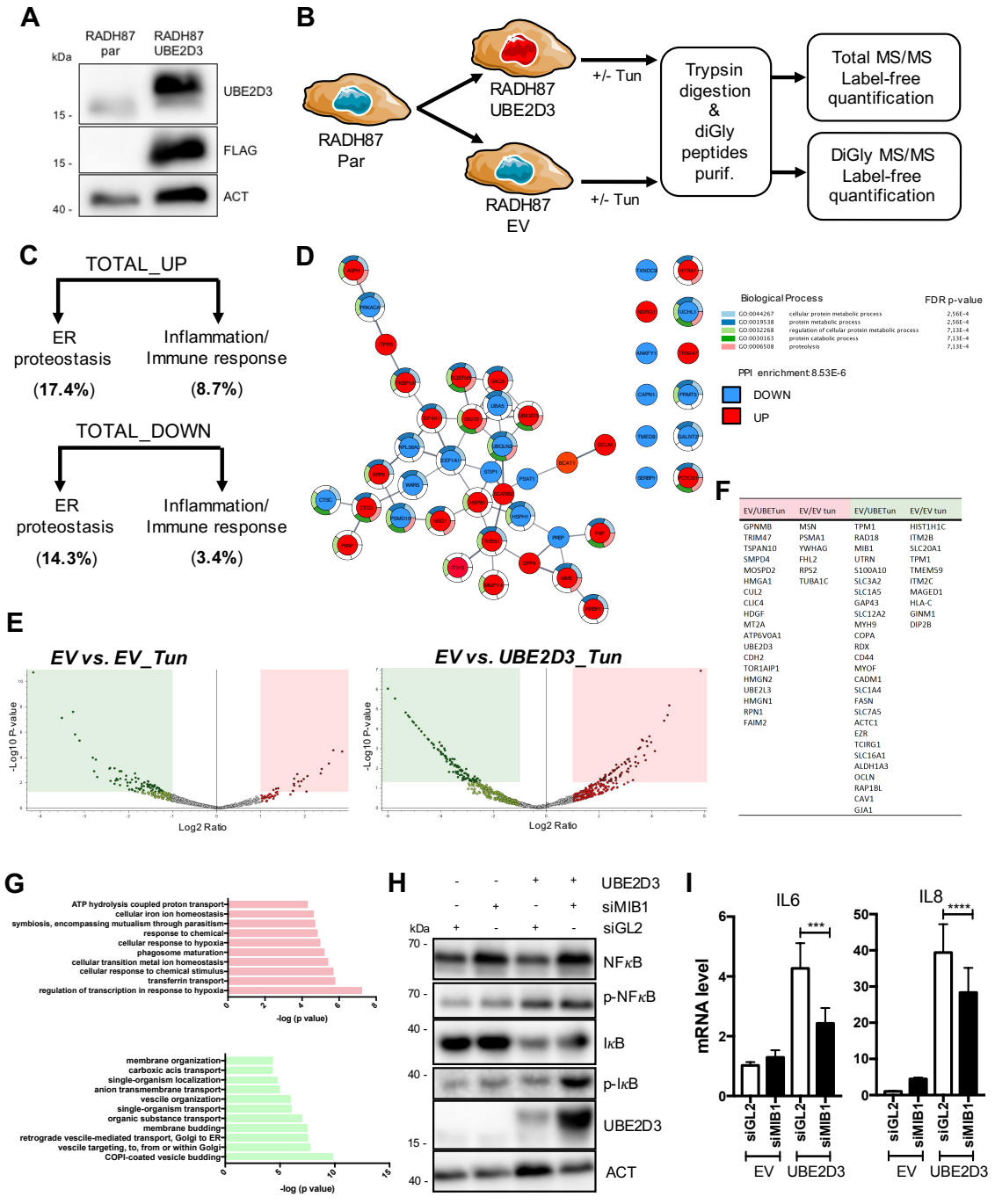

Figure 6